Inorg. Chem. **2005**, *44*, 4346–4358

Ligand Orientation Control in Low-Spin Six-Coordinate (Porphinato)iron(II) Species

Chuanjiang Hu,[†] Bruce C. Noll,[†] Charles E. Schulz,*[,‡] and W. Robert Scheidt*[,†]

Department of Chemistry and Biochemistry, University of Notre Dame, Notre Dame, Indiana 46556, and Department of Physics, Knox College, Galesburg, Illinois 61401

Received March 2, 2005

The synthesis of a low-spin six-coordinate iron(II) porphyrinate in which the two axial ligands are forced to have a relative perpendicular orientation has been successfully accomplished for the first time. The reaction of four-coordinate (tetramesitylporphinato)iron(II) with 2-methylimidazole leads to the preparation of [Fe(TMP)(2-MeHIm)$_2$] which cocrystallizes with five-coordinate [Fe(TMP)(2-MeHIm)]. The six-coordinate complex accommodates the sterically crowded pair of imidazoles with a strongly ruffled core and relative perpendicular orientation. This leads to shortened equatorial bonds of 1.963(6) Å and slightly elongated axial Fe–N bond lengths of 2.034(9) Å that are about 0.04 Å shorter and 0.03 Å longer, respectively, in comparison to those of the bis-imidazole-ligated iron(II) species with parallel oriented axial ligands. The Mössbauer spectrum shows a pair of quadrupole doublets that can be assigned to the components of the cocrystallized crystalline solid. High-spin five-coordinate [Fe(TMP)(2-MeHIm)] has $\Delta E_Q = 2.25$ mm/s and $\delta = 0.90$ mm/s at 15 K. The quadrupole splitting, ΔE_Q, for [Fe(TMP)(2-MeHIm)$_2$] is 1.71 mm/s, and the isomer shift is 0.43 mm/s at 15 K. The quadrupole splitting value is significantly larger than that found for low-spin iron(II) derivatives with relative parallel orientations for the two axial ligands. Mössbauer spectra thus provide a probe for ligand orientation when structural data are otherwise not available.

Introduction

Hemes (iron porphyrinate complexes) are the active component in many biologically important systems. These include the cytochrome *b* electron transfer proteins that are axially coordinated by two histidine ligands. For this case of heme centers coordinated to two planar histidine (imidazole) residues, there are a number of X-ray structures reported.[1−7] In each of these structures, it is found that an axial histidine plane is fixed in a particular orientation with respect to its projection onto the heme plane by a combination of the covalent attachment of the imidazole ring of the histidine residue to the protein backbone, hydrogen bonding of the imidazole N−H proton to the protein residues, and the packing of other amino acid side chains in the heme pocket. For bis-histidine-coordinated heme proteins, the relative orientation of the two imidazole planes with respect to each other is important for understanding the spectroscopic and also, possibly, the redox properties of these heme proteins. In the current protein structures, two limiting orientations of the axial ligand planes are found: (i) imidazole planes oriented parallel to each other (cytochromes b_5,[1] three of the heme centers of cytochromes c_3,[2−4] the *b* hemes of sulfite oxidase[5] and flavocytochrome b_2,[6] and the *a* heme of cytochrome oxidase[7]) and (ii) where one of the four heme groups in cytochrome c_3 from *Desulfovibrio vulgaris* has a more staggered conformation in which the dihedral angle between the histidine planes is closer to a relative perpendicular arrangement (77°).

* To whom correspondence should be addressed. E-mail: scheidt.1@nd.edu.
[†] University of Notre Dame.
[‡] Knox College.

(1) Mathews, F. S.; Czerwinski, E. W.; Argos, P. In *The Porphyrins*; Dolphin, D., Ed.; Academic Press: New York, 1979; Vol. VII, p 108.
(2) Pierrot, M.; Haser, R.; Frey, M.; Payan, F.; Astier, J.-P. *J. Biol. Chem.* **1982**, *257*, 14341.
(3) Higuchi, Y.; Kusunoki, M.; Matsuura, Y.; Yasuoka, N.; Kakudo, M. *J. Mol. Biol.* **1984**, *172*, 109.
(4) Czjzek, M.; Guerlesquin, F.; Bruschi, M.; Haser, R. *Structure* **1996**, *4*, 395.
(5) Kipke, C. A.; Cusanovich, M. A.; Tollin, G.; Sunde, R. A.; Enemark, J. H. *Biochemistry* **1988**, *27*, 2918.
(6) (a) Xia, Z.-X.; Shamala, N.; Bethge, P. H.; Lim, L. W.; Bellamy, H. D.; Xuong, N. H.; Lederer, F.; Mathews, F. S. *Proc. Natl. Acad. Sci. U.S.A.* **1987**, *84*, 2629. (b) Dubois, J.; Chapman, S. K.; Mathews, F. S.; Reid, G. A.; Lederer, F. *Biochemistry* **1990**, *29*, 6393.
(7) Iwata, S.; Ostermeier, C.; Ludwig, B.; Michel, H. *Nature* **1995**, *376*, 660.

10.1021/ic050320p CCC: $30.25
Published on Web 05/10/2005

There are also other bis-histidine-coordinated heme proteins believed to have their axial imidazole planes oriented perpendicular to each other. They have been identified largely on the basis of spectroscopic data for the oxidized (Fe(III)) forms and include the *b* hemes of mitochondrial complex III, also known as cytochrome bc_1,[8] the similar *b* hemes of cytochrome b_6f of chloroplasts, and the *c*-type heme of cytochrome *c*″ of *Methylophilus methylotrophus*.[9] For example, studies on cytochrome c_3[10] and *b* mitochondrial cytochromes[8b,11] have shown that changes in the relative orientations of the coordinated imidazole ligands cause significant changes of the observed *g* values for the low-spin complexes. These have large g_{max} EPR spectra[10,12−16] and a wider range of reduction potentials than those observed for cytochromes b_5 and b_2, and the *b* heme of sulfite oxidase, all of which have rhombic typical B hemichrome EPR spectra ($g_{zz} \sim 2.9-3.0$, $g_{yy} \sim 2.25-2.35$, $g_{xx} \sim 1.4-1.6$). Thus, there is a possibility of a correlation between the axial ligand plane orientation and the reduction potential in hemes and heme proteins.[15,17,18]

The orientations of planar axial ligands in bis-ligated hemes of iron(III) have been intensively investigated. The earliest studies showed that the relative and absolute orientations of the two axial ligands have significant effects on the electronic structure. The first example was [Fe(OEP)(3-ClPy)$_2$]ClO$_4$[19] for which two different crystalline polymorphs were isolated. The polymorphs are a triclinic spin-equilibrium system ($S = 1/2 \rightleftharpoons S = 5/2$)[20,21] and a monoclinic intermediate-spin system ($S = 3/2$).[22] In these complexes, the two pyridines maintained a relative parallel orientation but the absolute orientation of the two axial ligands with respect to the porphinato core changed. Although this system showed large changes in the electronic structure of iron(III), control of the axial ligand orientation is more likely to affect the relative energies of the three lowest d orbitals of iron, namely, the d_{xy}, d_{xz}, and d_{yz} orbitals.

While most bis-ligated iron(III) complexes have a characteristic rhombic EPR spectrum[23] with three observed *g* values, some iron(III) species have an unusual EPR spectrum: a single-feature low-spin EPR signal with $g \geq 3.2$. This EPR spectral type has been called the large g_{max}[24] or highly anisotropic low-spin (HALS)[25] EPR spectrum. The origin of the large g_{max} EPR spectrum was first studied in the complex [Fe(TPP)(2-MeHIm)$_2$]$^+$.[12,15] This study showed that the spectrum resulted from mutually perpendicular axial ligands that lead to nearly degenerate iron d_π orbitals. Subsequently, a number of additional iron(III) species were shown to have the two planar ligands oriented perpendicular to each other.[13,14,26−29] Most of these species display a large g_{max} EPR spectrum[13,14,16,27] and an unusually small value of the Mössbauer quadrupole splitting constant.[13−15,26,28,29] A final case was found for strong π-accepting ligands, such as 3- and 4-cyanopyridine, where the interaction with axial ligands lowers the energy of iron d_π orbitals below d_{xy} so that the ground state changes to $(d_{xz},d_{yz})^4(d_{xy})^1$. This leads to the final type of EPR spectrum observed in low-spin iron(III), an axial EPR spectrum. All of the complexes with relative perpendicular ligands are found to have strongly ruffled porphyrinato cores. For these systems, this conformation allows for the possibility of a π interaction between iron and the porphyrin.

In contrast to the comparative ease of obtaining relative perpendicular orientations of planar axial ligands in iron(III), iron(II) porphyrinates are found to display significantly different orientation behavior. The same strategies used with iron(II) porphyrinates yield bis-ligated species with relative parallel orientations.[30] Thus, for a series of substituted

(8) (a) Salerno, J. C. *J. Biol. Chem.* **1984**, *259*, 2331. (b) Tsai, A.; Palmer, G. *Biochim. Biophys. Acta* **1982**, *681*, 484. (c) Tsai, A.-H.; Palmer, G. *Biochim. Biophys. Acta* **1983**, *722*, 349.

(9) (a) Berry, M. J.; George, S. J.; Thomson, A. J.; Santos, H.; Turner, D. L. *Biochem. J.* **1990**, *270*, 413. (b) Costa, H. S.; Santos, H.; Turner, D. L.; Xavier, A. V. *Eur. J. Biochem.* **1992**, *208*, 427. (c) Costa, H. S.; Santos, H.; Turner, D. L. *Eur. J. Biochem.* **1993**, *215*, 817.

(10) Palmer, G. *Biochem. Soc. Trans.* **1985**, *13*, 548.

(11) Carter, K. R.; T'sai, A.-L.; Palmer, G. *FEBS Lett.* **1981**, *132*, 243.

(12) Scheidt, W. R.; Kirner, J. L.; Hoard, J. L.; Reed, C. A. *J. Am. Chem. Soc.* **1987**, *109*, 1963.

(13) Safo, M. K.; Gupta, G. P.; Walker, F. A.; Scheidt, W. R. *J. Am. Chem. Soc.* **1991**, *113*, 5497.

(14) Munro, O. Q.; Serth-Guzzo, J. A.; Turowska-Tyrk, I.; Mohanrao, K.; Shokhireva, T. Kh.; Walker, F. A.; Debrunner, P. G.; Scheidt, W. R. *J. Am. Chem. Soc.* **1999**, *121*, 11144.

(15) Walker, F. A.; Huynh, B. H.; Scheidt, W. R.; Osvath, S. R. *J. Am. Chem. Soc.* **1986**, *108*, 5288.

(16) Walker, F. A. *Chem. Rev.* **2004**, *104*, 589.

(17) Niki, K.; Kawasaki, Y.; Nishimura, N.; Higuchi, Y.; Yasuoka, N.; Kakudo, M. *J. Electroanal. Chem.* **1984**, *168*, 275.

(18) Nesset, M. J. M.; Shokhirev, N. V.; Enemark, P. D.; Jacobson, S. E.; Walker, F. A. *Inorg. Chem.* **1996**, *35*, 5188.

(19) The following abbreviations are used in this paper: Porph, a generalized porphyrin dianion; TMP, dianion of *meso*-tetramesitylporphyrin; T*p*-OCH$_3$PP, dianion of *meso*-tetra-*p*-methoxyphenylporphyrin; TPP, dianion of *meso*-tetraphenylporphyrin; TTP, dianion of *meso*-tetratolylporphyrin; TpivPP, dianion of α,α,α,α-tetrakis(*o*-pivalamidophenyl)porphyrin; Piv$_2$C$_8$P, dianion of α,α,5,15-[2,2′-(octanediamido)-diphenyl]-α,α,10,20-bis(*o*-pivalamidophenyl)porphyrin; TFPPBr$_8$, dianion of 2,3,7,8,12,13,17,18-octabromo-5,10,15,20-tetrakis(pentafluorophenyl)porphyrin; (C$_3$F$_7$)$_4$P, dianion of 5,10,15,20-tetrakis(heptafuoropropyl)porphyrin; Proto IX, dianion of protoporphyrin IX; *t*-Mu, dianion of *trans*-methylurocanate; *c*-Mu, dianion of *cis*-methylurocanate; OMTPP, dianion of octamethyltetraphenylporphyrin; OETPP, dianion of octaethyltetraphenylporphyrin; R-Im, a generalized hindered imidazole; HIm, imidazole; 1-MeIm, 1-methylimidazole; 2-MeHIm, 2-methylimidazole; 4-MeHIm, 4-methylimidazole; 5-MeHIm, 5-methylimidazole; 1,2-Me$_2$Im, 1,2-dimethylimidazole; 1-AcIm, 1-acetylimidazole; 1-SiMe$_3$Im, 1-(trimethylsilyl)imidazole; 1-VinIm, 1-vinylimidazole; 1-BzylIm, 1-benzylimidazole; Py, pyridine; 3-ClPy, 3-chloropyridine; 4-CNPy, 4-cyanopyridine; 3-CNPy, 3-cyanopyridine; 4-MePy, 4-methylpyridine; 3-EtPy, 3-ethylpyridine; 4-NMe$_2$Py, 4-(dimethylamino)pyridine; Pip, piperidine; pyz, pyrazine; N$_p$, porphyrinato nitrogen; Ct, center of four porphyrinato nitrogen atoms; N$_{Ax}$, nitrogen of axial ligands; N$_{im}$, nitrogen of imidazole ligands; C$_{im}$, carbon of imidazole ligands; Hb, hemoglobin; Mb, myoglobin; EPR, electron paramagnetic resonance.

(20) Scheidt, W. R.; Geiger, D. K. *J. Chem. Soc., Chem. Commun.* **1979**, 1154.

(21) Scheidt, W. R.; Geiger, D. K.; Haller, K. J. *J. Am. Chem. Soc.* **1982**, *104*, 495.

(22) Scheidt, W. R.; Geiger, D. K.; Hayes, R. G.; Lang, G. *J. Am. Chem. Soc.* **1983**, *105*, 2625.

(23) Blumberg, W. E.; Peisach, J. *Adv. Chem. Ser.* **1971**, *100*, 271.

(24) Walker, F. A.; Reis, D.; Balke, V. L. *J. Am. Chem. Soc.* **1984**, *106*, 6888.

(25) Magita, C. T.; Iwaizumi, M. *J. Am. Chem. Soc.* **1981**, *103*, 4378.

(26) Munro, O. Q.; Marques, H. M.; Debrunner, P. G.; Mohanrao, K.; Scheidt, W. R. *J. Am. Chem. Soc.* **1995**, *117*, 935.

(27) Inniss, D.; Soltis, S. M.; Strouse, C. E. *J. Am. Chem. Soc.* **1988**, *110*, 5644.

(28) Safo, M. K.; Gupta, G. P.; Watson, C. T.; Simonis, U.; Walker, F. A.; Scheidt, W. R. *J. Am. Chem. Soc.* **1992**, *114*, 7066.

(29) Safo, M. K.; Walker, F. A.; Raitsimring, A. M.; Walters, W. P.; Dolata, D. P.; Debrunner, P. G.; Scheidt, W. R. *J. Am. Chem. Soc.* **1994**, *116*, 7760.

pyridine derivatives, binding is independent of ligand basicity, and it was concluded that the insensitivity of the ligation behavior was the consequence of no interaction between the d_π orbitals of iron and the axial ligands. In addition, a series of imidazole-ligated iron(II) species in which the imidazoles are sterically unhindered showed relative parallel orientations for the two ligands.[31] Clearly iron(II) and iron(III) porphyrinates with two planar axial ligands have differing orientation preferences. This leads us to pose the following question: what are the electronic structure and orientation energy differences between the two oxidation states?

Another set of strategies used with great success in iron(III) to force relative perpendicular orientations is the use of sterically hindered imidazoles with a bulky 2-methyl substituent on the imidazole ring. However, for iron(II) systems, it is well-known that the use of sterically hindered imidazoles decreases the magnitude of the binding constant of the second imidazole, relative to those seen for unhindered imidazoles.[32] This leads the preparation and isolation of the high-spin five-coordinate species [Fe(Porph)(R-Im)].[33−35] However, [Fe(TPP)(2-MeHIm)] is reported to bind a second 2-methylimidazole ligand at low temperature,[36] which suggests that the synthesis of a bis-ligated hindered imidazole should be possible. Further encouragement for the successful synthesis was provided by the electrochemical measurement of the stability constants for iron(II) derivatives of tetraphenylporphyrin and tetramesitylporphyrin.[18] The presence of the bulky 2,6-methyl substituents in the iron(II) tetramesitylporphyrinate species led to an increased overall binding of two axial 2-methylimidazoles, confirming Safo's earlier qualitative observation.[37] However, despite these encouraging features, no synthesis or solid-state structure of a bis(2-methylimidazole) or related complex of an Fe(II) porphyrinate has yet appeared.

As part of our program to understand the control of iron(II) porphyrinate structure and the concomitant effect on physical properties, we have again tried to synthesize and isolate bis-ligated iron(II) porphyrinates with hindered imidazoles as the axial ligands. We have now successfully synthesized and structurally characterized the bis-ligated complex of the iron(II) derivative of tetramesitylporphyrin, [Fe(TMP)(2-MeHIm)$_2$]. The structure determination shows that the coordination of two 2-methylimidazole ligands leads to a low-spin iron(II) derivative with the two ligands having a relative perpendicular orientation. As expected from analogous iron(III) species, the porphyrin core is necessarily ruffled to accommodate the two ligands. Interestingly, the desired six-coordinate complex cocrystallized with the five-coordinate species [Fe(TMP)(2-MeHIm)]. The crystalline mixture has been characterized with the aid of Mössbauer spectroscopy, and full synthetic, structural, and Mössbauer details are presented herein.

Experimental Section

General Information. All reactions and manipulations for the preparation of the iron(II) porphyrin derivatives (see below) were carried out under argon using a double-manifold vacuum line, Schlenkware, and cannula techniques. Toluene and hexanes were distilled over sodium benzophenone ketyl. Methylene chloride was distilled over sodium hydride. Ethanethiol (Aldrich) was used as received. 2-Methylimidazole was purchased from Aldrich, recrystallized from toluene, and dried under vacuum. The free-base porphyrin ligand *meso*-tetramesitylporphyrin (H_2TMP) was prepared according to Lindsey et al.[38] The metalation of the free-base porphyrin to give [Fe(TMP)Cl] was done as previously described.[39] [Fe(TMP)](OH) was prepared according to a modified Fleischer preparation.[40] Mössbauer measurements were performed on a constant acceleration spectrometer from 15 to 300 K with optional small field (Knox College).

Synthesis of [Fe(TMP)(2-MeHIm)$_2$]. [Fe(TMP)(OH)] (0.04 mmol) was dissolved in 3 mL of methylene chloride, and 1 mL of ethanethiol was added by syringe. The mixture was stirred at room temperature for 3 days, and then a suspension of excess 2-methylimidazole (0.24 mmol) in 4 mL of hot toluene was added by cannula. The reaction mixture was then stirred for 1 h. X-ray quality crystals were obtained in 8 mm × 250 mm sealed glass tubes by liquid diffusion using hexanes as the nonsolvent after three weeks. Microcrystalline solids for the Mössbauer measurements were obtained by liquid diffusion in Schlenk tubes using hexanes as the nonsolvent. The solids were isolated in an inert-atmosphere box and immobilized in Apiezon M grease.

X-ray Structure Determination. A dark red crystal with the dimensions 0.20 × 0.26 × 0.33 mm^3 was used for the determination of the structure. The single-crystal experiment was carried out on a Bruker Apex system with graphite-monochromated Mo Kα radiation (λ = 0.71073 Å). The crystalline sample was placed in inert oil, mounted on a glass pin, and transferred to the cold gas stream of the diffractometer. Crystal data were collected at 100 K.

The structure was solved by direct methods using SHELXS-97[41] and refined against F^2 using SHELXL-97;[42,43] subsequent difference Fourier syntheses led to the location of most of the remaining non-hydrogen atoms. For the structure refinement all data

(30) Safo, M. K.; Nesset, M. J. M.; Walker, F. A.; Debrunner, P. G.; Scheidt, W. R. *J. Am. Chem. Soc.* **1997**, *119*, 9438.
(31) Safo, M. K.; Scheidt, W. R.; Gupta, G. P. *Inorg. Chem.* **1990**, *29*, 626.
(32) Rougee, M.; Brault, D. *Biochem. Biophys. Res. Commun.* **1974**, *57*, 654.
(33) Collman, J. P.; Reed, C. A. *J. Am. Chem. Soc.* **1973**, *95*, 2048.
(34) Collman, J. P.; Kim, N.; Hoard, J. L.; Lang, G.; Radonovich, L. J.; Reed, C. A. *Abstracts of Papers*, 167th National Meeting of the American Chemical Society, Los Angeles, CA, April 1974; American Chemical Society: Washington, DC, 1974; INOR 29.
(35) Ellison, M. K.; Schulz, C. E.; Scheidt, W. R. *Inorg. Chem.* **2002**, *41*, 2173.
(36) (a) Wagner, G. C.; Kassner, R. J. *J. Am. Chem. Soc.* **1974**, *96*, 5593. (b) Wagner, G. C.; Kassner, R. J. *Biochim. Biophys. Acta* **1975**, *392*, 319.
(37) Safo, M. K. Ph.D. Thesis, University of Notre Dame, Notre Dame, IN, 1991.
(38) Lindsey, J. S.; Wagner, R. W. *J. Org. Chem.* **1989**, *54*, 828.
(39) (a) Adler, A. D.; Longo, F. R.; Kampus, F.; Kim, J. *J. Inorg. Nucl. Chem.* **1970**, *32*, 2443. (b) Buchler, J. W. In *Porphyrins and Metalloporphyrins*; Smith, K. M., Ed.; Elsevier Scientific Publishing: Amsterdam, The Netherlands, 1975; Chapter 5.
(40) (a) Fleischer, E. B.; Srivastava, T. S. *J. Am. Chem. Soc.* **1969**, *91*, 2403. (b) Hoffman, A. B.; Collins, D. M.; Day, V. W.; Fleischer, E. B.; Srivastava, T. S.; Hoard, J. L. *J. Am. Chem. Soc.* **1972**, *94*, 3620.
(41) Sheldrick, G. M. *Acta Crystallogr.* **1990**, *A46*, 467.
(42) Sheldrick, G. M. *Program for the Refinement of Crystal Structures*; Universität Göttingen: Göttingen, Germany, 1997.

(43) $R_1 = \sum||F_o| - |F_c||/\sum|F_o|$ and $R_2 = \{\sum[w(F_o^2 - F_c^2)^2]/\sum[wF_o^4]\}^{1/2}$. The conventional R factor, R_1, is based on F with F set to zero for negative F^2. The criterion of $F^2 > 2\sigma(F^2)$ was used only for calculating R_1. R factors based on F^2 (R_2) are statistically about twice as large as those based on F, and R factors based on all of the data will be even larger.

were used, including negative intensities. The structure was refined as a racemic twin in space group $I\bar{4}$. The program SADABS[44] was applied for the absorption correction. Complete crystallographic details, atomic coordinates, bond distances and angles, anisotropic thermal parameters, and fixed hydrogen atom coordinates are given in the Supporting Information.

The asymmetric unit was found to contain four iron porphyrinate molecules as well as toluene, 2-methylimidazole, methylene chloride, water, and methanol solvates. Two of the iron porphyrinates are the desired bis-ligated species, [Fe(TMP)(2-MeHIm)$_2$]. These two molecules were completely ordered. These molecules will be termed mol 1 and mol 2. The third and fourth iron porphyrinates were five-coordinate species, [Fe(TMP)(2-MeHIm)] that had cocrystallized with the desired six-coordinate species. For the third iron molecule, [Fe(TMP)(2-MeHIm)] (mol 3), the axial 2-methylimidazole was found to be disordered over two positions, a major and a minor position, which were refined isotropically as rigid groups. The temperature factors of the atoms of the minor 2-methylimidazole [N(35b), N(36b), C(31b), C(32b), C(33b) and C(34b)] were constrained to be the same within an effective standard deviation (0.05). The occupancy of the major imidazole orientation was found to be 55%. For the fourth molecule, [Fe(TMP)(2-MeHIm)] (mol 4), both the iron and the 2-methylimidazole were found to be disordered over two positions (both sides of the porphyrin plane). Both 2-methylimidazoles were refined isotropically as rigid groups. A partially occupied methylene chloride molecule (occupancy is 0.20) is found in the same region as the minor 2-methylimidazole ligand. The occupancy of the major iron and 2-methylimidazole was found to be 68%. The atoms of other partially occupied methylene chloride, 2-methylimidazole, methanol, and water solvate molecules were refined isotropically. All other non-hydrogen atoms were refined anisotropically. For the porphyrin rings and the 2-methylimidazole ligands of mol 1 and mol 2, hydrogen atoms were added with the standard SHELXL-97 idealization methods; other hydrogen atoms were not generated. The largest residual density (2.4 e/Å^3) is 1.07 Å from Fe(3). Brief crystal data and intensity collection parameters for the crystalline complex are shown in Table 1, and complete details are given in Table S1.

Table 1. Crystallographic Details for [Fe(TMP)(2-MeHIm)$_2$]$_2$·[Fe(TMP)(2-MeHIm)]$_2$

formula	$C_{259.80}H_{259.85}Cl_{1.40}Fe_4N_{29.88}O_{0.76}$
unit cell content	8{[Fe(TMP)(2-MeHIm)$_2$]$_2$·[Fe(TMP)(2-MeHIm)]$_2$·$C_6H_5CH_3$·0.94(2-MeHIm)·0.7CH_2Cl_2·0.34CH_3OH·0.42H_2O}
fw, amu	4085.99
a, Å	39.8634(3)
c, Å	28.1013(6)
V, Å^3	44655.5(11)
space group	$I\bar{4}$
Z	8
D_c, g/cm^3	1.216
F(000)	1729
μ, mm^{-1}	0.334
cryst dimensions, mm	0.33 × 0.26 × 0.20
radiation	Mo Kα, $\bar{\lambda}$ = 0.71073 Å
temp, K	100(2)
total data collected	194984
abs correction	semiempirical from equivalents
unique data	44982 (R_{int} = 0.051)
unique observed data [$I > 2\sigma(I)$]	34716
refinement method	full-matrix least-squares on F^2
final *R* indices [$I > 2\sigma(I)$]	R_1 = 0.0632, R_2 = 0.1728
final *R* indices (all data)	R_1 = 0.0882, R_2 = 0.1903
absolute structure parameter	0.463(9)

Results

To obtain the bis-ligated iron(II) porphyrinates with two ligands oriented perpendicular to each other, we tried to synthesize bis-ligated Fe(II)(TMP) complexes with 2-methylimidazole or 1,2-dimethylimidazole as axial ligands. Many crystallization attempts were made with a variety of conditions and solvent to obtain good crystals. Finally, in the presence of toluene, methylene chloride, and ethanethiol, single crystals of [Fe(TMP)(2-MeHIm)$_2$] were obtained for 2-methylimidazole but not for 1,2-dimethylimidazole. In these crystals, we found that the asymmetric unit contains four independent porphyrin molecules. Surprisingly, two different species have cocrystallized: six-coordinate [Fe(TMP)(2-MeHIm)$_2$] (Figures 1 and 2) and five-coordinate [Fe(TMP)(2-MeHIm)] (Figures 3, S1, and S2). In these figures and in all of the tables, the following atom naming convention has been used: Q*(nyy)* where Q is the atom type, *n* refers to molecules 1−4, and *yy* are further numbers and letters needed to completely specify the atom. Similar atoms in the four molecules have the same name except for the digit *n*. Selected bond distances and angles are listed in Table 2.

The six-coordinate species have two imidazole ligands with a nearly perpendicular orientation. Equatorial bond distances (Fe−N_p) average 1.964(5) Å in mol 1 and 1.961(7) Å in mol 2. The axial bond lengths are 2.030(3) and 2.047(3) Å in [Fe(TMP)(2-MeHIm)$_2$] (mol 1), and 2.032(3) and 2.028(3) Å in [Fe(TMP)(2-MeHIm)$_2$] (mol 2).

The displacement of each atom of the porphyrin core from the 24-atom mean plane is shown in Figure 4. The orientations of the 2-MeHIm ligands, including the values of the dihedral angles, are also shown; the circle represents the position of the methyl group. Both six-coordinate species have significantly S_4-ruffled cores. The ligand planes make dihedral angles of 41.1° and 41.3° to the closest Fe−N_p axis in [Fe(TMP)(2-MeHIm)$_2$] (mol 1) and 44.8° and 37.9° in [Fe(TMP)(2-MeHIm)$_2$] (mol 2). This results in relative ligand orientations of 82.4° and 84.4° between the two imidazole

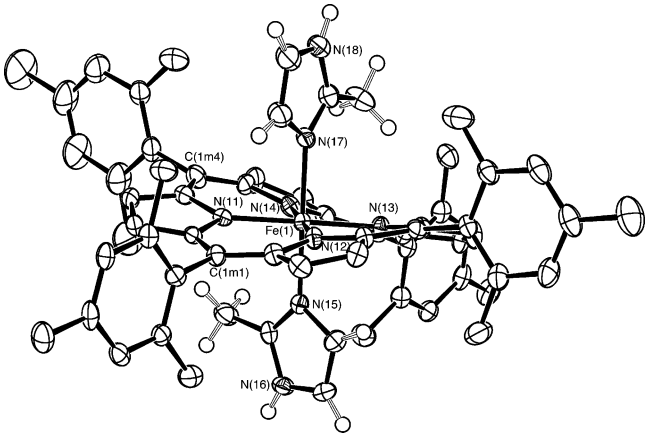

Figure 1. ORTEP diagram of six-coordinate [Fe(TMP)(2-MeHIm)$_2$] (mol 1). The hydrogen atoms of the porphyrin ligand have been omitted for clarity; the hydrogen atoms of the imidazole ligand are shown. Fifty percent probability ellipsoids are depicted.

(44) Sheldrick, G. M. *Program for Empirical Absorption Correction of Area Detector Data*; Universität Göttingen: Göttingen, Germany, 1996.

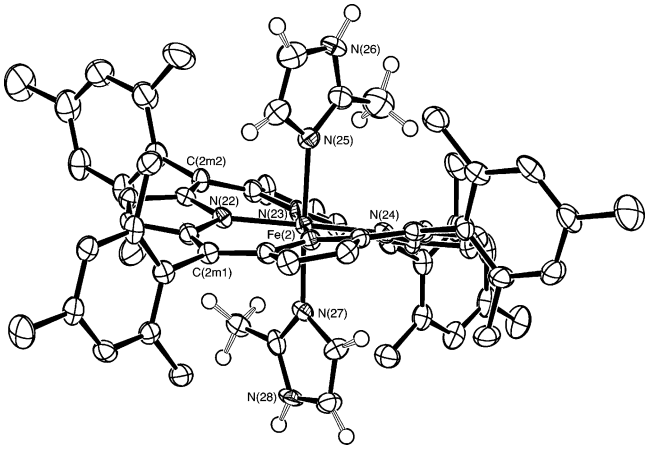

Figure 2. ORTEP diagram of six-coordinate [Fe(TMP)(2-MeHIm)$_2$] (mol 2) The hydrogen atoms of the porphyrin ligand have been omitted for clarity; the hydrogen atoms of the imidazole ligand are shown. Fifty percent probability ellipsoids are depicted. The orientations of the molecule in this figure and Figure 1 are chosen to show the similar conformations.

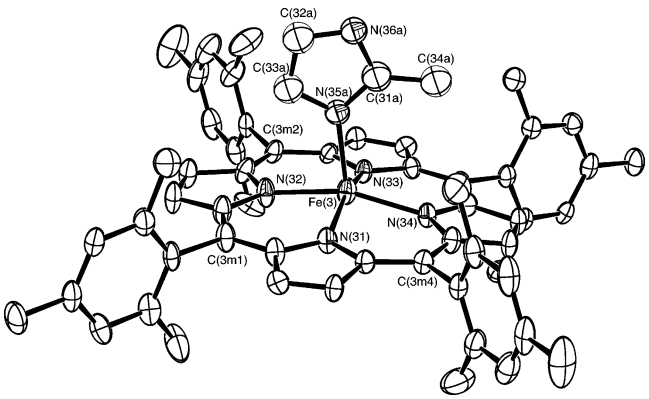

Figure 3. ORTEP diagram of [Fe(TMP)(2-MeHIm)] (mol 3). Only the major orientation (55%) of the imidazole ligand is shown. The hydrogen atoms have been omitted for clarity; 50% probability ellipsoids are depicted.

Table 2. Selected Bond Lengths and Angles for [Fe(TMP)(2-MeHIm)$_2$]$_2$·[Fe(TMP)(2-MeHIm)]$_2$

bond	length (Å)	bond	length (Å)
Fe(1)−N(11)	1.959(3)	Fe(1)−N(13)	1.961(3)
Fe(1)−N(12)	1.965(3)	Fe(1)−N(14)	1.971(3)
Fe(1)−N(15)	2.030(3)	Fe(1)−N(17)	2.047(3)
Fe(2)−N(24)	1.953(3)	Fe(2)−N(22)	1.958(3)
Fe(2)−N(23)	1.965(3)	Fe(2)−N(21)	1.969(3)
Fe(2)−N(27)	2.028(3)	Fe(2)−N(25)	2.032(3)
Fe(3)−N(31)	2.066(3)	Fe(3)−N(33)	2.066(3)
Fe(3)−N(34)	2.082(3)	Fe(3)−N(32)	2.084(3)
Fe(3)−N(35a)	2.123(4)	Fe(3)−N(35b)	2.204(5)
Fe(4a)−N(44)	2.062(3)	Fe(4a)−N(42)	2.065(4)
Fe(4a)−N(41)	2.073(3)	Fe(4a)−N(43)	2.104(3)
Fe(4a)−N(45a)	2.163(3)	Fe(4b)−N(42)	2.066(4)
Fe(4b)−N(44)	2.075(4)	Fe(4b)−N(43)	2.085(4)
Fe(4b)−N(45b)	2.117(9)	Fe(4b)−N(41)	2.131(4)

angle	value (deg)	angle	value (deg)
C(11)−N(15)−Fe(1)	132.0(3)	C(13)−N(15)−Fe(1)	122.2(3)
C(15)−N(17)−Fe(1)	133.0(3)	C(17)−N(17)−Fe(1)	120.6(3)
C(21)−N(25)−Fe(2)	133.7(3)	C(23)−N(25)−Fe(2)	119.2(3)
C(25)−N(27)−Fe(2)	133.2(3)	C(27)−N(27)−Fe(2)	121.6(3)
C(31a)−N(35a−-Fe(3)	127.1(3)	C(33a)−N(35a)−Fe(3)	126.4(3)
C(31b)−N(35b)−Fe(3)	127.9(4)	C(33b)−N(35b)−Fe(3)	124.5(4)
C(41a)−N(45a)−Fe(4a)	132.1(2)	C(43a)−N(45a)−Fe(4a)	120.3(2)

planes in mol 1 and mol 2, respectively. Both ligands are almost perpendicular to the porphyrin plane with dihedral

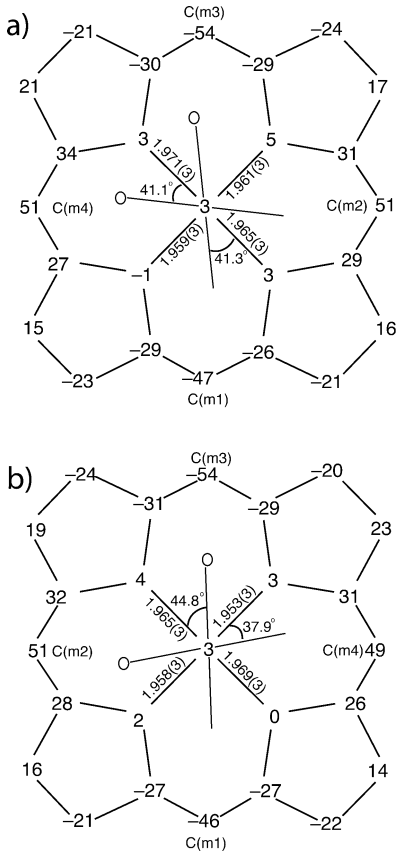

Figure 4. Formal diagrams of the porphyrinato cores of (a) [Fe(TMP)(2-MeHIm)$_2$] (mol 1) and (b) [Fe(TMP)(2-MeHIm)$_2$] (mol 2). The displacements of each atom from the 24-atom core plane in units of 0.01 Å are illustrated. The diagrams also show the orientation of the imidazole ligand with respect to the atoms of the porphyrin core. The position of the methyl group at the 2-carbon position is represented by the circle.

angles of 88.7° and 89.0° for [Fe(TMP)(2-MeHIm)$_2$] (mol 1) and 79.9° and 87.7° for [Fe(TMP)(2-MeHIm)$_2$] (mol 2).

Both five-coordinate [Fe(TMP)(2-MeHIm)] molecules are disordered. For mol 3, the 2-methylimidazole is disordered over two positions. Only the major position is displayed in Figure 3. For mol 4, both the iron and the 2-methylimidazole are disordered over two positions: above and below the porphyrin plane (Figure S2). The average Fe−N$_p$ distances are 2.074(10) and 2.076(19) Å in mol 3 and mol 4, respectively. The axial bond distances for the major imidazole orientation are 2.123(4) and 2.163(3) Å, respectively. As shown in Figure 5, the iron atom displacements from the 24-atom core are both 0.44 Å for the two five-coordinate species; this is a general feature of high-spin five-coordinate Fe(II) species. The Fe−N$_{im}$−C$_{im}$ angles are also listed in Table 2.

The Mössbauer spectra of the polycrystalline compound were taken at several different temperatures from 15 to 298 K. The observed spectra consist of two quadrupole doublets with equal area which, as will be discussed later, can be assigned to the two components of the polycrystalline derivative.

Discussion

Synthesis. One of our goals was to investigate if a six-coordinate Fe(II) porphyrin with hindered imidazole ligands

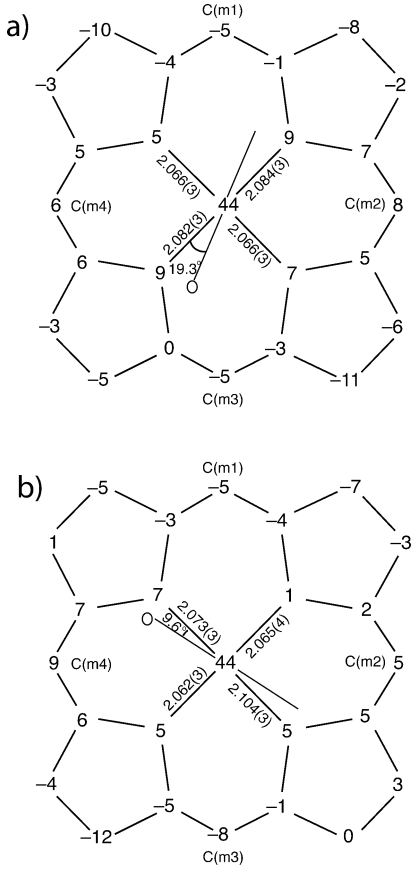

Figure 5. Formal diagrams of the porphyrinato cores of (a) [Fe(TMP)(2-MeHIm)] (mol 3) and (b) [Fe(TMP)(2-MeHIm)] (mol 4). The displacements of each atom from the 24-atom core plane in units of 0.01 Å are illustrated. The diagrams also show the orientation of the major imidazole ligand with respect to the atoms of the porphyrin core. The position of the methyl group at the 2-carbon position is represented by the circle.

could be synthesized and isolated. If such species could be synthesized, this would appear to be a strategy for controlling the relative axial ligand orientation in iron(II) species. Coordination of sterically hindered imidazoles as the axial ligand has been used as a strategy for synthesis of five-coordinate high-spin iron(II) porphyrins, as originally reported by Collman and Reed.[33] The strategy is based on the idea that the binding constant for adding the second axial ligand can be reduced by steric effects while not significantly affecting the binding of the first ligand for the equilibrium reactions below.[32]

$$\mathrm{Fe(Porph)} + \mathrm{L} \rightleftharpoons \mathrm{Fe(Porph)L} + \mathrm{L} \not\rightleftharpoons \mathrm{Fe(Porph)L_2}$$

However, the second binding constant K_2 is not reduced to a vanishingly small value with the use of hindered imidazoles. Thus, Kassner and Wagner[36] and later Brinigar et al.[45] showed, spectroscopically, that Fe(TPP) could bind two axial 2-methylimidazole ligands at low temperature. Safo[37] showed that the binding constant for the second 2-methylimidazole was porphyrin ligand dependent. Safo was able to spectroscopically demonstrate enhanced binding of the second axial ligand, even at ambient temperatures, when the porphyrin ligand was tetramesitylporphyrin. This particular porphyrin complex appeared to be a strong candidate for the preparation of a crystalline derivative. However, Safo was unable to prepare a solid crystalline species.[37]

After these experiments, Nesset et al.[18] measured, by electrochemical methods, the value of the second binding constant in DMF solution. They obtained a value of $\log(K_2) = 1.9$ for the iron(II) derivative of tetramesitylporphyrin and 2-methylimidazole for the reaction

$$\mathrm{Fe(TMP)L} + \mathrm{L} \rightleftharpoons \mathrm{Fe(TMP)L_2}$$

The equilibrium constant for binding the second hindered imidazole ligand is somewhat larger when the iron atom has been oxidized to the iron(III) oxidation state. Thus the low-spin iron(III) species, $[\mathrm{Fe(TPP)(2\text{-}MeHIm)_2}]^{+}$[12] and $[\mathrm{Fe(TMP)(1,2\text{-}Me_2Im)_2}]^{+}$,[26] have been isolated and structurally characterized. The complex $[\mathrm{Fe(OEP)(2\text{-}MeHIm)_2}]^{+}$,[46] also isolated and characterized, is a high-spin derivative. The steric effects of the hindering group are always a factor, and both the high-spin and low-spin species have (differing) structural features that minimize the nonbonded contacts between the hindering methyl group of the imidazole and the porphyrin core.

The relatively low value of the second binding constant (see equation below) shows part of the synthetic difficulty of preparing six-coordinate iron(II) derivatives

$$K_2 = \frac{[\mathrm{Fe(TMP)(L)_2}]}{[\mathrm{Fe(TMP)(L)}][\mathrm{L}]}$$

where L is 2-methylimidazole. Although the value of K_2 may be larger in some nonpolar solvents, the solubility of 2-methylimidazole limits our ability to drive the equilibrium toward complete formation of the six-coordinate species. Under our experimental conditions, [2-MeHIm] is about 0.03 mol/L, so the $[\mathrm{Fe(TMP)L_2}]/[\mathrm{Fe(TMP)L}]$ ratio is about 2.4 in the solution. Any crystallizing solution must thus contain a mixture of the five-coordinate and six-coordinate species. To obtain the pure crystalline six-coordinate complex, we needed to find a solvent system that favored its crystallization. The single crystals finally obtained for this system were formed in a solvent system of toluene, methylene chloride, and ethanethiol with hexane as the nonsolvent. In these crystals, the five-coordinate and six-coordinate species have *co*crystallized and have yielded an especially interesting structure.

$[\mathrm{Fe(TMP)(2\text{-}MeHIm)_2}]$ Structures. The asymmetric unit of the cell of the cocrystallized species contains four porphyrin molecules, two low-spin six-coordinate $[\mathrm{Fe(TMP)(2\text{-}MeHIm)_2}]$ molecules, and two high-spin five-coordinate [Fe(TMP)(2-MeHIm)] molecules. The low-spin state for $[\mathrm{Fe(TMP)(2\text{-}MeHIm)_2}]$ is evident from the structural parameters and from the Mössbauer studies described subsequently. With a confirmed low-spin state for the six-coordinate species, certain stereochemical features can be expected. The axial bonds to iron must be relatively short. A strongly ruffled

(45) Wang, C.-M.; Brinigar, W. S. *Biochemistry* **1979**, *18*, 4960.

(46) Geiger, D. K.; Lee, Y. J.; Scheidt, W. R. *J. Am. Chem. Soc.* **1984**, *106*, 6339.

porphyrin core is required in order to allow an appropriately close approach with the sterically bulky 2-methylimidazole ligands, with the formation of two oblong cavities at right angles on opposite sides of the porphyrin ring, and a relative perpendicular orientation of the two axial imidazole ligands. Both [Fe(TMP)(2-MeHIm)$_2$] mol 1 and mol 2 show such structural features. As can be seen from an examination of Figures 1 and 2, the two molecules have nearly identical core conformations and strongly similar relative and absolute axial ligand orientations. The absolute ligand orientation is given by the dihedral angle between the axial ligand plane and the closest $N_{ax}-Fe-N_p$ plane and is conventionally denoted by ϕ. The relative ligand orientation is simply the dihedral angle between the two axial ligand planes.

Additional quantitative information is given in Figure 4 which gives detailed displacements of each porphyrin core atom (in units of 0.01 Å from the 24-atom mean plane) and shows the orientation of the two axial ligands for each molecule. The figure also shows that the core conformations also display some (small) mixture of a saddling deformation. The steric interaction of the 2-methyl group adjacent to the coordinated nitrogen atom leads to a small tilting of the $Fe-N_{im}$ bond from the normal to the porphyrin plane: values are 3.0°, 3.5°, 3.5°, and 3.7°. The direction of the tilts always serves to decrease the imidazole methyl group···porphyrin core contacts. In addition, the methyl group leads to significantly different pairs of $Fe-N_{im}-C_{im}$ angles; the averaged angle involving the methyl side of imidazole is 133.0(7)°, while the unhindered C_{im} has $Fe-N_{im}-C_{im}$ average angles of 120.9(13)°. These are similar to those values in [Fe(TPP)(2-MeHIm)$_2$]$^{+12}$ where small tilt angles (∼4°) and large differences between two different $Fe-N_{im}-C_{im}$ angles are also observed.

The ligand binding pocket is bounded by the 2- and 6-methyl substituents of the peripheral mesityl substituents. The ruffling of the core leads to large variation in the position of the 2- and 6-methyl substituents with respect to the mean plane of the porphyrin core. There are effectively two classes of methyl groups: one group has an average perpendicular distance of 1.51 Å from the mean porphyrin plane, while the second has an average distance of 3.29 Å. These are clearly visible in Figures 1 and 2. These features are similar to those observed in a number of iron(III) derivatives of TMP and have been previously described.[13] These conformational features result in the dihedral angles between the mesityl groups and the core all being nearly 90°. The observed dihedral angles are 88.0°, 89.5°, 82.1°, and 81.7° in [Fe(TMP)(2-MeHIm)$_2$] (mol 1) and 90.0°, 86.9°, 89.0°, and 77.8° in [Fe(TMP)(2-MeHIm)$_2$] (mol 2).

The generally observed value for the equatorial $Fe-N_p$ distances in low-spin six-coordinate iron(II) porphyrinates is ∼2.000 Å, ∼0.01 Å longer than than those observed for comparable iron(III) species.[47] These complexes have effectively planar porphyrin core conformations. The average

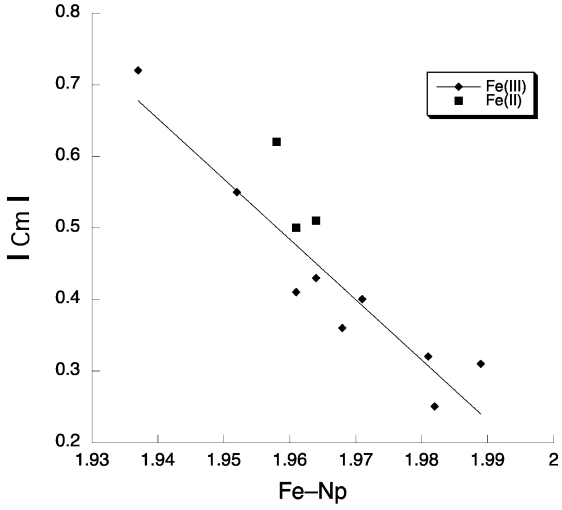

Figure 6. Plot of absolute *meso*-carbon (C_m) displacement (Å) vs the $Fe-N_p$ bond distance (Å) for iron(II) and iron(III) porphyrinates with two axial ligands perpendicular to each other.

equatorial distances observed in [Fe(TMP)(2-MeHIm)$_2$] are shorter at 1.964(5) (mol 1) and 1.961(7) Å (mol 2); the observed decrease (bond shortening) is the clear result of the core ruffling.

Some time ago, Hoard[48,49] pointed out that there should be a quantitative relationship between the degree of core ruffling and the amount of bond shortening. The shortenings observed for the [Fe(TMP)(2-MeHIm)$_2$] derivatives are in general agreement with those expectations. We have explored the issue more quantitatively by examining the value of the equatorial $Fe-N_p$ bond distances with the degree of ruffling in iron(II) and iron(III) derivatives. All such ruffled derivatives are axially ligated by two planar ligands with relative perpendicular orientations. We take the average absolute displacement of the methine carbon atoms (C_m) from the mean plane of the 24-atom core as a quantitative measure of the ruffling of the core. A plot of average absolute C_m displacements against the equatorial $Fe-N_p$ bond distance in the known iron(III) derivatives[12−14,26−29,63] is given in Figure 6; detailed values are given in Table 3.[50−64] The C_m displacements vary from 0.25 to 0.72 Å, and the $Fe-N_p$ distances correspondingly range from 1.989 to 1.937 Å. The line illustrated is the best fit to these iron(III) data. The two values for [Fe(TMP)(2-MeHIm)$_2$] and the one other iron(II) datum[55,65] available from the literature (shown with filled

(47) Scheidt, W. R. Systematics of the Stereochemistry of Porphyrins and Metalloporphyrins. In *The Porphyrin Handbook*; Kadish, K. M., Smith, K., Guilard, R., Eds.; Academic Press: San Diego, CA, 2000; Vol. 3, Chapter 16.

(48) Hoard, J. L. *Ann. N.Y. Acad. Sci.* **1973**, *206*, 18.
(49) Collins, D. M.; Scheidt, W. R.; Hoard, J. L. *J. Am. Chem. Soc.* **1972**, *94*, 6689.
(50) Li, N.; Petricek, V.; Coppens, P.; Landrum, J. *Acta Crystallogr.* **1985**, *C41*, 902.
(51) Li, N.; Coppens, P.; Landrum, J. *Inorg. Chem.* **1988**, *27*, 482.
(52) Hiller, W.; Hanack, M.; Mezger, M. G. *Acta Crystallogr.* **1987**, *C43*, 1264.
(53) Radonovich, L. J.; Bloom, A.; Hoard, J. L. *J. Am. Chem. Soc.* **1972**, *94*, 2074.
(54) Grinstaff, M. W.; Hill, M. G.; Birnbaum, E. R.; Schaefer, W. P.; Labinger, J. A.; Gray, H. B. *Inorg. Chem.* **1995**, *34*, 4896.
(55) Moore, K. T.; Fletcher, J. T.; Therien, M. J. *J. Am. Chem. Soc.* **1999**, *121*, 5196.
(56) Scheidt, W. R.; Osvath, S. R.; Lee, Y. J. *J. Am. Chem. Soc.* **1987**, *109*, 1958.
(57) Silver, J.; Marsh, P. J.; Symons, M. C. R.; Svistunenko, D. A.; Frampton, C. S.; Fern, G. R. *Inorg. Chem.* **2000**, *39*, 2874.

Table 3. Selected Bond Distances (Å) and Angles (deg) for [Fe(TMP)(2-MeHIm)$_2$] (mol 1 and mol 2) and Related Species[a]

Iron(II)

complex	Fe−N$_p$[b,c]	Fe−N$_{Ax}$[c]	C$_m$[c,d]	ϕ[e,f]	relative orientation[e,g]	ref
[Fe(TMP)(2-MeHIm)$_2$] (mol 1)	1.964(5)	2.030(3)	0.51	41.1	82.4	this work
		2.047(3)		41.4		
[Fe(TMP)(2-MeHIm)$_2$] (mol 2)	1.961(7)	2.032(3)	0.50	44.8	84.4	this work
		2.028(3)		37.9		
[Fe(TPP)(1-VinIm)$_2$]	2.001(2)	2.004(2)		14	0[h]	31
[Fe(TPP)(1-BzylIm)$_2$]	1.993(9)	2.017(4)		26	0[h]	31
[Fe(TPP)(1-MeIm)$_2$]	1.997(6)	2.014(5)		15	0[h]	31
[Fe(TMP)(4-CNPy)$_2$]	1.992(1)	1.996(2)		40	0[h]	30
[Fe(TMP)(3-CNPy)$_2$]	1.996(0)	2.026(2)		42	0[h]	30
[Fe(TMP)(4-MePy)$_2$]	1.988(0)	2.010(2)		41	0[h]	30
[Fe(TPP)(Py)$_2$]·2Py	1.993(6)	2.039(1)		34.4	0[h]	50
[Fe(TPP)(Py)$_2$]	2.001(2)	2.037(1)		45	0[h]	51
[Fe(TPP)(Pip)$_2$]	2.004(6)	2.127(3)			0[h]	53
[Fe(TPP)(pyz)$_2$]	1.987(8)	1.990(28)		3.9/37.0	40.9	52
[Fe(TFPPBr$_8$)(Py)$_2$]	1.963(4)	2.012(7)			90	54
[Fe((C$_3$F$_7$)$_4$P)(py)$_2$]	1.958(4)	2.002(11)	0.62	41.3/46.0	87.5	55

Iron(III)

complex	Fe−N$_p$[b,c]	Fe−N$_{Ax}$[c]	C$_m$[c,d]	ϕ[e,f]	relative orientation[e,g]	ref
[Fe(TMP)(1-MeIm)$_2$]ClO$_4$	1.988(20)	1.975(3)		23	0[h]	13
	1.987(1)	1.965(3)		41	0[h]	
[Fe(TPP)(HIm)$_2$]Cl·CHCl$_3$	1.994(12)	1.977(3)		6	0[h]	56
	1.993(4)	1.964(3)		41	0[h]	
[Fe(TPP)(4-MeHIm)$_2$]Cl	2.000(11)	1.975(2)		3.1	0[h]	57
	1.995(10)	1.987(2)		4.6	0[h]	57
[Fe(TPP)(*t*-Mu)$_2$]SbF$_6$	1.992(5)	1.983(4)		22	0[h]	58
[Fe(TPP)(*c*-Mu)$_2$]SbF$_6$	1.997(1)	1.967(7)		29	0[h]	58
	1.995(17)	1.979(7)		15	0[h]	
[Fe(TPP)(1-MeIm)$_2$]ClO$_4$	1.982(11)	1.974(6)[b]		22/32	11	60
[Fe(OEP)(4-NMe$_2$Py)$_2$]ClO$_4$	2.002(4)	1.995(3)		36	0[h]	13
[Fe(Proto IX)(1-MeIm)$_2$]	1.991(16)	1.977(16)[b]		3/16	13	61
paral-[Fe(TMP)(5-MeHIm)$_2$]ClO$_4$	1.983(4)	1.970(12)[b]		10/46	30	14
	1.981(5)	1.982(3)[b]		14/12	26	
paral-[Fe(OMTPP)(1-MeIm)$_2$]Cl	1.990(2)	1.996(29)[b]	0.01	12.6/6.9	19.5	62
[Fe(TPP)(HIm)$_2$]Cl·MeOH	1.989(8)	1.974(24)[b]	0.31	18/39	57	63
perp-[Fe(TMP)(5-MeHIm)$_2$]ClO$_4$	1.981(7)	1.965(11)[b]	0.32	30/12	76	14
[Fe(TPP)(2-MeHIm)$_2$]ClO$_4$	1.971(4)	2.012(4)[b]	0.40	32/32	89.3	12
[Fe(TMP)(1,2-Me$_2$Im)$_2$]ClO$_4$	1.937(12)	2.004(0)[b]	0.72	44.8/45.4	89.4	26
[Fe(TPP)(Py)$_2$]ClO$_4$	1.982(7)	2.003(3)[b]	0.25	34/38	86	27
[Fe(TMP)(3-ClPy)$_2$]ClO$_4$	1.968(3)	2.012(8)[b]	0.36	48/29	77	28
[Fe(TMP)(4-CNPy)$_2$]ClO$_4$	1.961(7)	2.011(14)[b]	0.41	43/44	90	29
[Fe(TMP)(3-EtPy)$_2$]ClO$_4$	1.964(4)	1.996(9)[b]	0.43	43/43	90	28
[Fe(TMP)(4-NMe$_2$Py)$_2$]ClO$_4$	1.964(10)	1.984(8)[b]	0.51	37/42	79	13
[Fe(TPP)(4-CNPy)$_2$]ClO$_4$	1.952(7)	2.002(8)[b]	0.55	35/36	89	29
perp-[Fe(OMTPP)(1-MeIm)$_2$]Cl	1.969(7)	1.982(10)	0.10	29.3	90.0[h]	62
[Fe(OETPP)(1-MeIm)$_2$]Cl	1.970(7)	1.977(1)[b]	0.03	9.6/82.7	73	62
[Fe(OETPP)(4-NMe$_2$Py)$_2$]Cl	1.951(5)	2.000(22)[b]	0.28	9.0/29.0	70	64
[Fe(OMTPP)(4-NMe$_2$Py)$_2$]ClO$_4$	1.979(3)	2.009[b]	0.01	1.3/2.4	84.2	78
[Fe(OMTPP)(Py)$_2$]ClO$_4$	1.973(3)	2.024(4)	0.18	23.4	90.0[h]	78
[Fe(OETPP)(4-NMe$_2$Py)$_2$]ClO$_4$	1.977(2)	2.030(3)[b]	0.08	10.6/20.5	53.2	78

[a] Estimated standard deviations are given in parentheses. [b] Averaged value. [c] In angstroms. [d] Average absolute values of the displacements of the methine carbons from the 24-atom mean plane. [e] Value in degrees. [f] Dihedral angle between the plane defined by the closest N$_p$−Fe−N$_{im}$ and the imidazole plane. [g] Dihedral angle between two axial ligands. [h] Exact value required by symmetry.

squares) are also shown in Figure 2. The figure suggests not only a strong correlation between the degree of ruffling and the equatorial bond distance shortening but also that the small difference (∼0.01 Å) between the iron(II) and iron(III) porphyrinate Fe−N$_p$ bond distances remains when the derivatives have ruffled conformations.

It is to be noted that one of the two bis(pyridine) derivatives of iron(II) with nearly relative perpendicular pyridine ligands displayed in Table 3 is not shown in Figure 6. The core conformation of [Fe(TFPPBr$_8$)(Py)$_2$][54] is saddled as a result of the peripheral steric congestion. [Fe((C$_3$F$_7$)$_4$P)-

(58) Quinn, R.; Valentine, J. S.; Byrn, M. P.; Strouse, C. E. *J. Am. Chem. Soc.* **1987**, *109*, 3301.
(59) Hatano, K.; Safo, M. K.; Walker, F. A.; Scheidt, W. R. *Inorg. Chem.* **1991**, *30*, 1643.
(60) Higgins, T.; Safo, M. K.; Scheidt, W. R. *Inorg. Chim. Acta* **1990**, *178*, 261.
(61) Little, R. G.; Dymock, K. R.; Ibers, J. A. *J. Am. Chem. Soc.* **1975**, *97*, 4532.
(62) Yatsunyk, L. A.; Carducci, M. D.; Walker, F. A. *J. Am. Chem. Soc.* **2003**, *125*, 15986.
(63) Collins, D. M.; Countryman, R.; Hoard, J. L. *J. Am. Chem. Soc.* **1972**, *94*, 2066.
(64) Ogura, H.; Yatsunyk, L.; Medforth, C. J.; Smith, K. M.; Barkigia, K. M.; Renner, M. W.; Melamed, D.; Walker, F. A. *J. Am. Chem. Soc.* **2001**, *123*, 6564.
(65) The other possible iron(II) derivative listed in Table 3 has a saddled core conformation.

Table 4. Selected Bond Distances and Angles for [Fe(TMP)(2-MeHIm)$_2$] (mol 3 and mol 4) and Related Species[a]

complex	Fe−N$_p$[b,c]	Fe−N$_{im}$[c]	ΔN$_4$[c,d]	Δ[c,e]	C···N[c]	Fe−N−C[f,g]	Fe−N−C[f,h]	θ[f,i]	φ[f,j]	ref
[Fe(TMP)(2-MeHIm)] (mol 3)	2.074(10)	2.123(4)[k]	0.36	0.44	2.042	127.1(3)	126.4(3)	9.1	19.3	this work
[Fe(TMP)(2-MeHIm)] (mol 4)	2.076(19)	2.163(3)[k]	0.40	0.44	2.038	132.2(2)	120.2(2)	5.2	9.6	this work
[Fe(TPP)(1,2-Me$_2$Im)]	2.079(8)	2.158(2)[k]	0.36	0.42	2.048	129.3(2)	124.9(2)	11.4	20.9	67
[Fe(TTP)(2-MeHIm)]	2.076(3)	2.144(1)	0.32	0.39	2.050	132.8(1)	121.4(1)	6.6	35.8	67
[Fe(T*p*-OCH$_3$PP)(2-MeHIm)]	2.087(7)	2.155(2)[k]	0.39	0.51	2.049	130.4(2)	123.4(2)	8.6	44.5	67
[Fe(T*p*-OCH$_3$PP)(1,2-Me$_2$Im)]	2.077(6)	2.137(4)	0.35	0.38	2.046	131.9(3)	122.7(3)	6.1	20.7	67
[Fe(TPP)(2-MeHIm)] (2-fold)	2.086(8)	2.161(5)	0.42	0.55	2.044	131.4(4)	122.6(4)	10.3	6.5	34
[Fe(TPP)(2-MeHIm)]·1.5C$_6$H$_5$Cl	2.073(9)	2.127(3)[k]	0.32	0.38	2.049	131.1(2)	122.9(2)	8.3	24.0	35
[Fe(TpivPP)(2-MeHIm)]	2.072(6)	2.095(6)	0.40	0.43	2.033	132.1(8)	126.3(7)	9.6	22.8	68
[Fe(Piv$_2$C$_8$P)(1-MeIm)]	2.075(20)	2.13(2)	0.31	0.34	2.051	126.5	120.4	5.0	34.1	69

[a] Estimated standard deviations are given in parentheses. [b] Averaged value. [c] In angstroms. [d] Displacement of the iron from the mean plane of the four pyrrole nitrogen atoms. [e] Displacement of the iron from the 24-atom mean plane of the porphyrin core. [f] Value in degrees. [g] Imidazole 2-carbon, sometimes methyl substituted. [h] Imidazole 4-carbon. [i] Off-axis tilt (deg) of the Fe−N$_{im}$ bond from the normal to the porphyrin plane. [j] Dihedral angle between the plane defined by the closest N$_p$ −Fe−N$_{im}$ and the imidazole plane in degrees. [k] Major imidazole orientation.

(py)$_2$],[55] on the other hand, has a ruffled core that is thought to be a result of the bulky *meso*-C$_3$F$_7$ groups. Although the basis for the ruffling may be different, the compound follows the ruffling pattern.

The average value of the four axial Fe−N$_{im}$ distances is 2.034(9) Å which is slightly longer than the corresponding distances observed in other bis(imidazole-ligated) iron(II) porphyrinates with unhindered imidazoles (2.004 Å in [Fe(TPP)(1-VinIm)$_2$], 2.017 Å[31] in [Fe(TPP)(1-BzylIm)$_2$],[31] and 2.014 Å in [Fe(TPP)(1-MeIm)$_2$])[66] where the two ligand planes have a relative parallel orientation. Thus, the steric crowding from the methyl group leads to a small increase in the axial Fe−N bond distance of about 0.02 Å. As shown in Table 3, the differences in axial bond lengths between hindered and unhindered imidazoles in the iron(III) derivatives appear to be a bit larger, but all of the iron(III) distances are shorter than those of iron(II), reflecting the effects of the oxidation state of iron.

[Fe(TMP)(2-MeHIm)] Structures. The structural features of the two five-coordinate [Fe(TMP)(2-MeHIm)] species have the common features found in other high-spin imidazole-ligated Fe(II) porphyrinates.[34,35,67] These include an expanded porphinato core, large equatorial Fe−N$_p$ bond distances, and a significant out-of-plane displacement of the iron(II) atom. Selected structural parameters for related high-spin iron(II) derivatives are given for comparison in Table 4.[68,69] The similarities between the known structures and the two new molecules are evident. As shown in Figure 5, both five-coordinate species show core conformations with doming and some ruffling. The extent of the doming is given by the difference between the displacement of the iron atom from the four nitrogen atoms (ΔN$_4$) and the mean plane of the 24-atom core (Δ); the values are not unusual.

The imidazole 2-methyl group adjacent to the coordinated nitrogen atom creates a steric interaction with the porphyrin core and leads to a tilting of the Fe−N$_{im}$ bond from the normal to the porphyrin plane. For these five-coordinate species, the tilt angles are 5.2° and 9.1°. There are also two types of Fe−N$_{im}$−C$_{im}$ angles that serve to minimize the steric interactions. Despite the presence of the hindering methyl group, the dihedral angles between the imidazole plane and the nearest N$_p$−Fe−N$_{im}$ plane are 19.3° and 9.6°. The orientation of the imidazole is also shown in Figure 5.

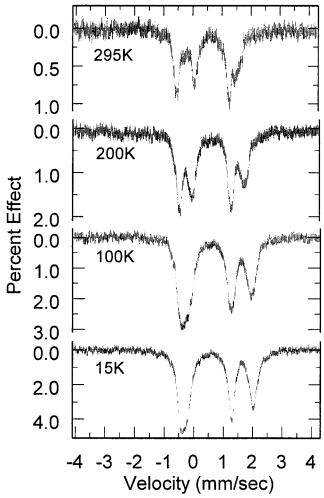

Figure 7. Solid-state Mössbauer spectra at several different temperatures. Lines are numbered from 1 to 4 from left to right and are clearly seen in the spectrum at 200 K.

Mössbauer Spectra. Mössbauer spectra were measured from room temperature to 15 K. The spectra consist of two quadrupole doublets that are overlapped at most temperatures; spectra are illustrated in Figure 7. The two doublets have equal area as would be expected for a crystalline species that shows 1:1 stoichiometry of the two cocrystallized species. The isomer shift (δ) and quadrupole splitting (ΔE_q) values have been obtained by fitting these data to a set of four Lorentzian lines. The pairwise assignment of lines into quadrupole doublets is based on the temperature dependence of the isomer shift. Only with the assignments of lines 1 and 3 as a doublet and lines 2 and 4 as a second doublet does one get a proper monotonic decrease of the two isomer shift values with increasing temperature. Complete results from the fitting of the temperature-dependent data are given in Tables 5 and 6. One of the doublets has a strongly temperature-dependent quadrupole splitting with values of

(66) Steffen, W. L.; Chun, H. K.; Hoard, J. L.; Reed, C. A. *Abstracts of Papers*, 175th National Meeting of the American Chemical Society, Anaheim, CA, March 13, 1978; American Chemical Society: Washington, DC, 1978; INOR 15.
(67) Hu, C.; Roth, A.; Ellison, M. K.; An, J.; Ellis, C. M.; Schulz, C. E.; Scheidt, W. R. *J. Am. Chem. Soc.* **2005**, *127*, 5675.
(68) Jameson, G. B.; Molinaro, F. S.; Ibers, J. A.; Collman, J. P.; Brauman, J. I.; Rose, E.; Suslick, K. S. *J. Am. Chem. Soc.* **1980**, *102*, 3224.
(69) Momenteau, M.; Scheidt, W. R.; Eigenbrot, C. W.; Reed, C. A. *J. Am. Chem. Soc.* **1988**, *110*, 1207.

Table 5. Mössbauer Parameters for Five-Coordinate [Fe(TMP)(2-MeHIm)] and Related Complexes

complex	ΔE_Q[a]	δ_{Fe}[a]	*T*, K	ref
[Fe(TMP)(2-MeHIm)]	2.25	0.90	15	this work
	2.21	0.90	50	this work
	2.12	0.90	100	this work
	1.78	0.84	200	this work
	1.46	0.79	298	this work
[Fe(T*p*-OCH_3PP)(1,2-Me_2Im)]	2.47	0.94	16	67
	2.28	0.92	50	
	2.27	0.92	100	
	2.10	0.91	150	
	1.97	0.88	200	
	1.88	0.90	250	
	1.77	0.81	298	
	−2.44	0.95	4.2	
[Fe(T*p*-OCH_3PP)(2-MeHIm)]	−2.18	0.94	4.2	67
[Fe(TPP)(1,2-Me_2Im)]	−1.93	0.92	4.2	67
[Fe(TPP)(2-MeHIm)]	−1.96	0.86	4.2	67
[Fe(TTP)(2-MeHIm)]	−1.95	0.85	4.2	67
[Fe(TTP)(1,2-Me_2Im)]	−2.06	0.86	4.2	67
[Fe(TPP)(2-MeHIm)]	−2.40	0.92	4.2	35
[Fe(TPP)(2-MeHIm)(2-fold)	−2.28	0.93	4.2	70
[Fe(TPP)(1,2-Me_2Im)]	−2.16	0.92	4.2	70
Hb	−2.40	0.92	4.2	70
Mb	−2.22	0.92	4.2	70

[a] In millimeters per second.

ΔE_q that range from 1.46 to 2.25 mm/s and isomer shift values that range from 0.79 mm/s at room temperature to 0.90 mm/s at 15 K. These values are reasonable for five-coordinate high-spin Fe(II) porphyrinates.[35,67,70] Table 5 shows the strong similarity between the Mössbauer data observed for the current complex (five-coordinate [Fe(TMP)(2-MeHIm)]) and related species. The large temperature dependence of the quadrupole splitting is presumably caused by the presence of close-lying excited states of the same or lower spin multiplicity and appears to be a general feature of all five-coordinate imidazole-ligated iron(II) porphyrinates.

The second quadrupole doublet comes from the six-coordinate [Fe(TMP)(2-MeHIm)$_2$] component of the crystals. The [Fe(TMP)(2-MeHIm)$_2$] data are given at the top of Table 6; the values of the quadrupole splitting and isomer shift vary only slightly with temperature. The isomer shift value is that expected for a low-spin iron(II) complex. However, the quadrupole splitting value of ∼1.70 mm/s is significantly larger than those previously measured for bis(imidazole) complexes as crystalline solids. The comparison with the Mössbauer data given in Table 6 is generally shown at a temperature chosen to facilitate comparisons; a few systems have values shown at two temperatures. None of the iron(II) species of Table 6, when such data are available, show significant temperature dependence of quadrupole splitting. Nearly all of the other species whose Mössbauer spectra have been obtained with the species as crystalline solids have known structures. In all of these structures, save that of [Fe(TMP)(2-MeHIm)$_2$], the two axial ligands are in a relative parallel configuration; the absolute orientations show a wide range of ϕ values (values in Table 3). We can thus conclude that the quadrupole splitting value for low-spin bis(planar axial ligand) iron(II) systems is sensitive to the relative orientation of the two axial ligands. Larger values of the quadrupole splitting (≥1.5 mm/s) indicate the presence of a relative perpendicular orientation for the two axial ligands, while lower values (≤1.25 mm/s) indicate relative parallel orientations. Frozen solution Mössbauer data for Fe(TMP) in the presence of a hindered imidazole have also been obtained. These data are shown in the top portion of Table 6; the values of quadrupole splitting are totally consistent with the conclusion that derivatives with perpendicular relative orientations have large values for quadrupole splitting. It is to be noted that the dependence of the magnitude of quadrupole splitting with ligand orientation in the iron(II) derivatives is the opposite of that observed for the iron(III) derivatives. In the iron(III) derivatives, the species with relative perpendicular ligand orientations have the small values for quadrupole splitting. Thus, any explanation for the pattern seen in the iron(II) derivatives must also be able to account for the pattern in the iron(III) derivatives.

From Table 6, we see an interesting contrast between [Fe(TMP)(2-MeHIm)$_2$] and the other bis-ligated Fe(II) compounds of known molecular structure: only [Fe(TMP)(2-MeHIm)$_2$] has a ruffled core conformation, whereas the remaining iron(II) derivatives have effectively planar porphyrin cores. Concomitantly, only [Fe(TMP)(2-MeHIm)$_2$] has a perpendicular relative orientation for the two planar axial ligands; the remainder have relative parallel orientations.

One theoretical framework for understanding the origins of the quadrupole splitting involves the dominant contributions to the electric field gradient (EFG) from the 3d electrons. The valence electron contribution to the EFG can be expressed by the Townes-Dailey approximation[75]

$$q_{val} = \frac{4}{5}\langle r^{-3}\rangle\left[-N(p_z) + \frac{1}{2}(N(p_x) + N(p_y))\right] + \frac{4}{7}\langle r^{-3}\rangle\left[N(d_{x^2-y^2}) - N(d_{z^2}) + N(d_{xy}) - \frac{1}{2}(N(d_{xz}) + N(d_{yz}))\right] \quad (1)$$

where N(p) and N(d) are the effective populations of the appropriate 4p and 3d iron orbitals, respectively, and $\langle r^{-3}\rangle$ is the expectation value of $1/r^3$ taken over the appropriate 3d and 4p radial functions.

For low-spin 3d^6 complexes, the t_2 orbitals (d_{xz}, d_{yz}, d_{xy}) are all nominally doubly occupied. If that were strictly the case, their net contribution to the EFG would be zero. And for our purposes, with a positive quadrupole splitting,[76] we need an explanation of why the d_π orbitals (which make

(70) Kent, T. A.; Spartalian, K.; Lang, G.; Yonetani, T.; Reed, C. A.; Collman, J. P. *Biochim. Biophys. Acta* **1979**, *580*, 245.

(71) Kobayashi, H.; Maeda, Y.; Yanagawa, Y. *Bull. Chem. Soc. Jpn.* **1970**, *43*, 2342.

(72) Dolphin, D.; Sams, J. R.; Tsin, T. B.; Wong, K. L. *J. Am. Chem. Soc.* **1976**, *98*, 6970.

(73) Polam, J. R.; Wright, J. L.; Christensen, K. A.; Walker, F. A.; Flint, H.; Winkler, H.; Grodzicki, M.; Trautwein, A. X. *J. Am. Chem. Soc.* **1996**, *118*, 5272.

(74) Epstein, L. M.; Straub, D. K.; Maricondi, C. *Inorg. Chem.* **1967**, *6*, 1720.

(75) (a) Bancroft, G. M.; Mays, M. J.; Prater, B. E. *J. Chem. Soc. A* **1970**, 956. (b) Bancroft, G. M.; Platt, R. H. *Adv. Inorg. Chem. Radiochem.* **1972**, *15*, 59. (c) Grodzicki, M.; Männing, V.; Trautwein, A. X.; Freidt, J. M. *J. Phys. B: At., Mol. Opt. Phys.* **1987**, *21*, 5595. (d) Paulsen, H.; Ding, X.-Q.; Grodzicki, M.; Butzlaff, Ch.; Trautwein, A. X.; Hartung, R.; Wieghardt, K. *Chem. Phys.* **1994**, *184*, 149.

Table 6. Mössbauer Parameters for Six-Coordinate [Fe(TMP)(2-MeHIm)$_2$] and Related Species

Fe(II) Complexes

complex	ΔE_Q[a]	δ_{FE}[a]	sample phase	*T*, K	relative orientation[b]	conf[c]	ref
[Fe(TMP)(2-MeHIm)$_2$]	1.71	0.43	cryst solid	15	82.4/84.4	ruf	this work
	1.70	0.42		50			this work
	1.70	0.42		100			this work
	1.76	0.40		200			this work
	1.78	0.35		298			this work
[Fe(TPP)(1-MeIm)$_2$]	1.07	0.47	cryst solid	77	0	pla	31
[Fe(TPP)(1-AcIm)$_2$]	0.97	0.45	cryst solid	77	*d*	*d*	31
[Fe(TPP)(1-VinIm)$_2$]	1.02	0.45	cryst solid	77	0	pla	31
[Fe(TPP)(1-BzylIm)$_2$]	1.02	0.45	cryst solid	77	0	pla	31
[Fe(TPP)(1-SiMe$_3$Im)$_2$]	1.04	0.46	cryst solid	77	*d*	*d*	31
[Fe(TPP)(Py)$_2$]	1.15	0.40	cryst solid	77	0	pla	71
[Fe(OEP)(Py)$_2$]	1.13	0.46	cryst solid	4.2	*d*	*d*	72
[Fe(TMP)(1-MeIm)$_2$]	1.11	0.43	cryst solid	120	*d*	*d*	30
	1.09	0.45		4.2			
[Fe(TMP)(4-CNPy)$_2$]	1.13	0.41	cryst solid	120	0	pla	30
	1.11	0.42		4.2			
[Fe(TMP)(3-ClPy)$_2$]	1.23	0.43	cryst solid	120	0	pla	30
	1.24	0.45		4.2			
[Fe(TMP)(4-MePy)$_2$]	1.12	0.42	cryst solid	120	0	pla	30
	1.09	0.43		4.2			
[Fe(TMP)(4-NMe$_2$Py)$_2$]	1.27	0.36	cryst solid	120	0	pla	30
	1.20	0.39		4.2			
[Fe(TMP)(2-MeHIm)$_2$]	1.64	0.39	frozen soln	77	*e*	*e*	73
[Fe(TMP)(1,2-Me$_2$Im)$_2$]	1.73	0.39	frozen soln	77	*e*	*e*	73
[Fe(OEP)(2-MeHIm)$_2$]	1.67	0.34	frozen soln	77	*e*	*e*	73
[Fe(OEP)(4-NMe$_2$Py)$_2$]	1.02	0.45	frozen soln	77	*d*	*d*	73
[Fe(OEP)(4-CNPy)$_2$]	1.10	0.32	frozen soln	77	*d*	*d*	73
[Fe(OEP)(1-MeIm)$_2$]	0.96	0.46	frozen soln	77	*d*	*d*	73

Fe(III) Complexes

complex	ΔE_Q[a]	δ_{FE}[a]	sample phase	*T*, K	relative orientation[b]	conf[c]	ref
[Fe(TMP)(4-NMe$_2$Py)$_2$]ClO$_4$	1.74	0.20	cryst solid	77	79	ruf	13
perp-[Fe(TMP)(5-MeHIm)$_2$]ClO$_4$	1.78	0.22	cryst solid	120	76	ruf	14
[Fe(TPP)(2-MeHIm)$_2$]ClO$_4$	1.77	0.22	cryst solid	120	89.3	ruf	15
[Fe(TMP)(1,2-Me$_2$Im)$_2$]ClO$_4$	1.26	0.17	cryst solid	120	89.4	ruf	26
[Fe(TMP)(2-MeHIm)$_2$]ClO$_4$	1.48	0.20	cryst solid	77	*e*	*e*	28
[Fe(TMP)(3-EtPy)$_2$]ClO$_4$	1.25	0.18	cryst solid	77	90	ruf	28
[Fe(TMP)(3-ClPy)$_2$]ClO$_4$	1.36	0.20	cryst solid	77	77	ruf	28
[Fe(TPP)(Py)$_2$]Cl	1.25	0.16	solid	77	*e*	*e*	74
[Fe(TMP)(4-CNPy)$_2$]ClO$_4$	0.97	0.20	cryst solid	77	70	ruf	28
[Fe(TPP)(4-CNPy)$_2$]ClO$_4$	0.65	0.19	cryst solid	4.2	89	ruf	29
perp-[Fe(OMTPP)(1-MeIm)$_2$]Cl	1.76		cryst solid		90	sad	16
[Fe(OETPP)(1-MeIm)$_2$]Cl	1.94		cryst solid		73	sad	16
[Fe(OETPP)(4-NMe$_2$Py)$_2$]Cl	1.89		cryst solid		70	sad	16
[Fe(OMTPP)(4-NMe$_2$Py)$_2$]ClO$_4$	1.89	0.23	cryst solid	70	84	sad	78
[Fe(OMTPP)(Py)$_2$]ClO$_4$	2.18	0.25	cryst solid	78	90	sad	78
[Fe(OETPP)(4-NMe$_2$Py)$_2$]ClO$_4$	2.31	0.26	cryst solid	80	53,70	sad	78,64
paral-[Fe(TMP)(5-MeHIm)$_2$]ClO$_4$	2.56	0.22	cryst solid	120	26/30	pla	14
[Fe(TMP)(1-MeHIm)$_2$]ClO$_4$	2.28	0.28	cryst solid	77	0	pla	13
[Fe(OEP)(4-NMe$_2$Py)$_2$]ClO$_4$	2.14	0.26	cryst solid	77	0	pla	13
[Fe(TPP)(4-MeHIm)$_2$]Cl	2.26	0.34	cryst solid	77	0	pla	57
[Fe(TPP)(HIm)$_2$]Cl	2.23	0.23	crystalline(?)	77	*d*	*d*	74
paral-[Fe(OMTPP)(1-MeIm)$_2$]Cl	2.80		cryst solid		19.5	sad	16

[a] In millimeters per second. [b] Dihedral angle between two axial ligands. [c] Predominant core conformation contribution: pla, planar; ruf, ruffled; and sad, saddled. [d] Not determined, presumed parallel and planar. [e] Not determined, presumed perpendicular and ruffled.

negative contributions to the EFG) have smaller populations than the d_{xy} orbital, and the populations are even smaller in a ruffled porphyrin than in a more planar one.

Grodzicki et al.[77] have done some theoretical calculations that are helpful. Their results show that for both [Fe(TMP)(1-MeIm)$_2$] and [Fe(TMP)(2-MeHIm)$_2$] the energies of the d orbitals have the following order: $d_{yz} < d_{xz} < d_{xy} < d_{z^2} < d_{x^2-y^2}$. The splitting between the d_π states is very small (0.006 and 0.018 eV for the two compounds, respectively). Furthermore, the population of the d_{xy} orbital is very similar in the two compounds (1.982 and 1.988) and is larger than the population of d_{xz} (1.740 and 1.859) and d_{yz} (1.758 and 1.805). The latter two orbital populations are, in fact, slightly smaller for the relative perpendicular ligand plane orientations than for relative parallel ligand plane orientations. But even more significantly, Grodzicki did model calculations on two structures with hindered perpendicular imidazoles, one with a planar porphyrin core and one with a ruffled porphyrin core. The populations of the d_π orbitals were significantly smaller with the ruffled porphyrin core thus predicting a larger quadrupole splitting.

(76) We were not able to assign the sign of the quadrupole splitting from our data because the multiple lines of the two components in the magnetic Mössbauer spectrum mixture will make assignments difficult or impossible. However, solution measurements for [Fe(TMP)(2-MeHIm)$_2$] and [Fe(TMP)(1-MeIm)$_2$] at 4.2 K have established positive signs for the quadrupole splitting for both.[77]

(77) Grodzicki, M.; Flint, H.; Winkler, H.; Walker, F. A.; Trautwein, A. X. *J. Phys. Chem. A* **1997**, *101*, 4202.

As described in the structure section, the six-coordinate Fe(II) complex has shortened Fe−N_p bonds that correlate with the strong ruffling. We suggest the shorter Fe−N_p bonds enhance the π interaction between Fe($3d_\pi$) and $N_p(2p_\pi)$. The stronger π interaction will cause Fe → N_π donation, lowering $N(d_{xz})$ and $N(d_{yz})$. The resulting reduction of the negative contributions to the EFG ($N(d_{xz})$ and $N(d_{yz})$) results in the observed larger quadrupole splitting.

It is interesting to observe (Table 6) that while for Fe(II) complexes the quadrupole splitting is higher for the ruffled porphyrins with perpendicular ligand planes than for planar porphyrins with parallel ligands, the opposite is true in Fe(III) complexes. That observation calls for an explanation as well. Among the bis-ligated Fe(III) compounds, we can identify three structural/spectroscopic categories: (type I) perpendicular ligands, normally with a ruffled or saddled porphyrin core, a large g_{max} EPR, and quadrupole splittings in the range of 1.24−1.78 mm/s; (type II) parallel ligands, usually with a planar porphyrin core, although a saddled example exists, a classic rhombic EPR, and quadrupole splittings in the range of 2.14−2.8 mm/s; and (type III) nearly perpendicular axial ligands, with a ruffled porphyrin core, an axial EPR spectrum, and a very small quadrupole splitting ($\leq$1.00 mm/s).

Our goal is to understand the systematics of these categories and how the resulting structures allow us to make sense of the measured EPR and Mössbauer parameters. In particular, the quadrupole splittings are interesting, as the largest splittings for the Fe(III) models occur with parallel ligands, while for Fe(II) models, the splitting is larger for perpendicular ligands.

The EPR differences between the three groups are understood in terms of the d electron configuration differences that depend on which t_2 orbital is singly occupied (highest in energy), as determined by the crystal field of the ligands. The d_{xy} orbital is singly occupied in type III compounds; this conclusion is based on the fact that, in the Taylor formalism,[79] a negative tetragonal crystal field is required to fit the observed g values so that the d_{xy} orbital moves above both of the d_π orbitals in energy and thus becomes singly occupied. In the Townes-Dailey approximation, the valence contribution to the EFG should be proportional to

$$\Delta N(d) = N(d_{x^2-y^2}) + N(d_{xy}) - N(d_{z^2}) - (N(d_{xz}) + N(d_{yz}))/2 \quad (2)$$

Type III compounds have roughly one more d_π electron and one fewer d_{xy} electron than types I and II. Both of these changes will reduce the EFGs for type III compounds; therefore, the small quadrupole splitting values observed are to be expected.

Type I compounds have a singly occupied d_π orbital and, on the basis of the g values, must have a relatively weak rhombic crystal field which, in turn, implies that the two d_π orbitals will be close in energy and therefore strongly mixed by spin−orbit coupling. This results in the characteristic large g_{max} EPR spectrum. Type II compounds also have an unpaired d_π electron, but in contrast to type I, they exhibit classic rhombic EPR spectra. The g values of such spectra imply that the rhombic crystal fields for type II compounds are much larger than those for type I species. Therefore, the ground d_π orbital has much smaller mixtures of the other two t_2 orbitals. It is reasonable that the rhombic crystal field should be larger for members of this group because the parallel configuration of the ligand planes will result in a much larger asymmetry between the x and y axes than for the perpendicular-plane configuration of type I.

We understand why types I and II should have larger quadrupole splittings than type III, but explaining why type II shows larger quadrupole splittings than type I is harder. The key to understanding this effect is to note that, for the ruffled and saddled hemes, the symmetry is lowered so that the porphyrin π^* orbitals can mix with the iron d_{xy} orbital. In this case, π donation out of the doubly occupied d_{xy} will occur in distorted porphyrins, while it is symmetry forbidden in the planar complexes. The smaller $N(d_{xy})$ for type I compounds, as can be seen in eq 2, results in a smaller quadrupole splitting for these compounds than for type II compounds.

In type II species with parallel ligand planes and $\phi \approx 0$, the axial nitrogen π orbitals have the right symmetry to mix with the iron d_π orbitals and compete with any possible bonding between the iron and porphyrin π orbitals. This competition makes it a challenge to determine if iron will be a net acceptor or donor as a result of these π interactions. Toward this end, we note the following: (i) It is reasonable to assume that, for $\phi \approx 0$, the singly occupied d orbital (d_{yz}) is likely to be along the axis of the imidazole. (ii) It has also been noted[56] that, for [Fe(TPP)$(HIm)_2$]Cl, the equatorial Fe−N_p bonds perpendicular to the imidazole plane are shorter than the parallel bonds. These points are consistent with the idea that the doubly occupied d_{xz} orbital has increased π donation to the porphyrin π system. The fact that most complexes with relative parallel ligands also have a value of ϕ near zero argues that π interaction with iron is significant. There may well also be π donation from the imidazole into the iron orbitals. To assess the net effect on the quadrupole splitting, we would need a theoretical calculation to determine if the result of the π interactions is an increase or decrease of the population of the iron d_π orbitals.

We see that the quadrupole splitting seems to be slightly larger for those planar models having relative orientations slightly greater than zero (Table 6). This distortion from axial parallel alignment is expected to reduce the π interaction with the axial ligands, and the larger quadrupole splitting is consistent with reduced π donation from those ligands.

We note in Tables 3 and 6 that for some of the compounds both parallel and perpendicular arrangements of the axial ligands are possible. Also, for the same ligands, the use of different porphyrins can change the orientation from parallel to perpendicular (e.g., [Fe(TMP)$(4\text{-}NMe_2Py)_2$]ClO_4 vs [Fe(OEP)$(4\text{-}NMe_2Py)_2$]ClO_4). A natural conclusion is that

(78) Ohgo, Y.; Ikeue, T.; Takahashi, M.; Takeda, M.; Nakamura, M. *Eur. J. Inorg. Chem.* **2004**, *798*, 5034.
(79) Taylor, C. P. S. *Biochim. Biophys. Acta* **1977**, *491*, 137.

the transitions between the various structural forms are rather delicately poised and may be driven one way or another by small effects such as crystal packing forces. In this case, the solid-state EPR and Mössbauer spectra are very likely to differ from those one would obtain in a frozen solution.

Summary. The synthesis and isolation of a six-coordinate low-spin iron(II) porphyrinate with its axial ligands in a relative perpendicular orientation has been accomplished for the first time. The porphyrin core is strongly ruffled, consistent with the necessary use of a hindered imidazole to achieve a relative perpendicular orientation. The complex has been characterized by an X-ray diffraction study. The equatorial $Fe-N_p$ bonds are shorter than those found in analogous planar complexes that have the two axial imidazoles in a relative parallel orientation. However, the axial $Fe-N_{im}$ bonds are longer than when the ligands are oriented in a relative perpendicular orientation. As a result of the relatively low binding constant for the addition of the sixth ligand, the desired complex, [Fe(TMP)(2-MeHIm)$_2$], co-crystallizes with the five-coordinate precursor. Nonetheless, the study shows that a perpendicular orientation of axial ligands is experimentally accessible. The complex mixture has been characterized by variable temperature Mössbauer spectroscopy. The Mössbauer quadrupole splitting constants of the complexes with relative perpendicular orientations are significantly larger than those of derivatives with similar axial ligands, and they show that the Mössbauer quadrupole splitting constant can be used to evaluate the relative ligand orientation of bis-ligated iron(II) porphyrinates.

Acknowledgment. We thank the National Institutes of Health for support of this research under Grant GM-38401. C.E.S. thanks Prof. T. Clayton for helpful discussions.

Supporting Information Available: Tables S1−S6 which give complete crystallographic details, atomic coordinates, bond distances and angles, anisotropic temperature factors, and fixed hydrogen atom positions, Figure S1 which shows the two disordered axial imidazole ligands in [Fe(TMP)(2-MeHIm)] (mol 3), Figure S2 which shows the two disordered parts of iron and imidazole in [Fe(TMP)(2-MeHIm)] (mol 4) (PDF), and an X-ray crystallographic file in CIF format. This material is available free of charge via the Internet at http://pubs.acs.org.

IC050320P